Scientific Reports

https://doi.org/10.1038/s41598-026-49377-3

Article in Press

Transcranial vibrotactile stimulation enhances hippocampal cholinergic signaling and memory through frequency-dependent mechanotransduction

Received: 11 December 2025

Accepted: 14 April 2026

Published online: 22 April 2026

Cite this article as: Kim O., Shin C., Cho M. *et al.* Transcranial vibrotactile stimulation enhances hippocampal cholinergic signaling and memory through frequency-dependent mechanotransduction. *Sci Rep* (2026). https://doi.org/10.1038/s41598-026-49377-3

Ok-Hyeon Kim, Chang-Ho Shin, Min-Woo Cho, Jae-Young Ha, Jai Jun Choung, Dong-Keun Song, Jae-Yeong Choi, Eun Seo Chang, Hyun Jung Lee & Sae-Kwang Ku

Transcranial vibrotactile stimulation enhances hippocampal cholinergic signaling and memory through frequency-dependent mechanotransduction

Ok-Hyeon Kim[1†], Chang-Ho Shin[2,3†], Min-Woo Cho[3], Jae-Young Ha[3], Jai Jun Choung[3], Dong-Keun Song[3] Jae-Yeong Choi [4], Eun Seo Chang[5], Hyun Jung Lee[1,5*], Sae-Kwang Ku[6*]

[1] Department of Anatomy and Cell Biology, College of Medicine, Chung-Ang University, Seoul, 06974, Republic of Korea

[2] Department of AI Convergence Biomedical Engineering, Dongguk University, Goyang-si, 10326, Republic of Korea

[3] AriBio Co., Ltd., 56 Dongpangyo-ro, Bundang-gu, Seongnam-si, 13535, Republic of Korea.

[4] Evosonics Co., Ltd., 42-10, Taejanggongdan-gil, Wonju-si, Gangwon-do, 26311, Republic of Korea

[5] Department of Global Innovative Drugs, Graduate School of Chung-Ang University, Seoul, 06974, Republic of Korea

[6] Department of Anatomy and Histology, College of Korean Medicine, Daegu Haany University, Gyeongsan, 38610, Republic of Korea.

[†]equally contributed first authors

*correspondence to Hyun Jung Lee, Ph.D., (pluto38@cau.ac.kr) and Sae-Kwang Ku, Ph.D. (gucci200@dhu.ac.kr)

Ok-Hyeon Kim: ssimba315@cau.ac.kr

Chang-Ho Shin: changhoshin84@gmail.com

Min-Woo Cho: mwcho@aribio.com

Jae-Young Ha: jyha@aribio.com

Jai Jun Choung: mchoung@aribio.com

Dong-Keun Song: dksong@aribio.com

Jae-Yeong Choi: choi@evosonics.com

Eun Seo Chang: amy2069@cau.ac.kr

Hyun Jung Lee: pluto38@cau.ac.kr

Sae-Kwang Ku: gucci200@hanmail.net, gucci200@dhu.ac.kr

ORCID number

Ok-Hyeon Kim: 0000-0001-6496-1669

Chang-Ho Shin: 0009-0002-5848-4485

Dong-Keun Song: 0000-0002-9238-3816

Hyun Jung Lee: 0000-0002-9941-9826

Sae-Kwang Ku: 0000-0003-1269-3804

Abstract

Cholinergic dysfunction is a key contributor to cognitive impairment observed in aging and neurodegenerative disorders such as Alzheimer's disease (AD). Although acetylcholinesterase (AChE) inhibitors have been the mainstay of symptomatic treatment for over two decades, their limited efficacy and adverse effects underscore the need for alternative therapeutic approaches. Recent evidence indicates that mechanical stimulation can modulate neuronal and glial signaling through mechanotransduction, suggesting a potential strategy to enhance cognitive function via non-pharmacological means.

Here, we developed a head-mounted vibrotactile stimulation system (HVSS) that delivers controlled vibration to the cranium and evaluated its effects in a pharmacological model of acute cholinergic dysfunction induced by scopolamine. To this end, male C57BL/6 mice received scopolamine (1 mg/kg, i.p.; on days 7, 14, and 28) and were exposed to daily vibrotactile stimulation at 20, 40, or 80 Hz for 28 days. Behavioral performance was assessed using passive avoidance and Morris water maze tests, followed by biochemical and histological analyses. HVSS at 40 Hz and 80 Hz significantly improved cognitive performance, enhanced hippocampal cholinergic function, reduced oxidative damage, and upregulated memory-related signaling genes, including *BDNF*, *PI3K*, *AKt*, *ERK1/2*, *CREB*, and *CAMK4*.

These findings suggest that high-frequency HVSS improves memory hippocampal cholinergic function via activation of memory-related signaling pathways, highlighting its potential as a safe, non-pharmacological neuromodulatory strategy for cholinergic dysfunction-related cognitive decline.

Keywords Vibrotactile stimulation, Cognitive decline, Cholinergic dysfunction, Oxidative stress, Mechanotransduction

Word count: (150-250) 217

Introduction

Cognitive decline and memory impairment are major features of aging and neurodegenerative disease, with Alzheimer's disease (AD) being the most prevalent[1]. One of the critical neurochemical alterations underlying these conditions is cholinergic dysfunction, characterized by the loss of cholinergic neurons in the basal forebrain and subsequent reduction in acetylcholine (ACh) levels in the hippocampus and cortex[2]. The disruption of cholinergic signaling leads to impaired synaptic transmission and cognitive deficits commonly observed in AD and age-related cognitive disorders. ACh is synthesized by choline acetyltransferase (ChAT)[3], and hydrolyzed by acetylcholinesterase (AChE), which terminates cholinergic neurotransmission. Although AChE inhibitors such as tacrine, donepezil, and rivastigmine have been used for symptomatic treatment[1], their benefits are modest and transient, and adverse effects, including hepatotoxicity, often limit their use[4,5]. Over the past two decades, no pharmacological intervention has shown durable efficacy in modifying disease progression except for a few recently approved monoclonal antibodies against amyloid beta[6,7]. However, these antibody therapies provide only partial slowing of cognitive decline and carry safety and accessibility concerns, reflecting the multifactorial and complex nature of AD pathogenesis and underscoring the need for alternative treatments with improved safety profiles.

Mechanical stimulation, including vibrotactile stimulation, can modulate cellular activity and neurophysiological functions by converting mechanical forces into biochemical responses through mechanotransduction processes that influence intracellular signaling and neuronal plasticity[8]. Recent studies have highlighted that biomechanical forces in the aging brain contribute to cognitive decline and AD pathology by affecting interstitial fluid dynamics, neuroinflammation, and neuronal network activity [9]. Moreover, mechanical or

sensory stimulation at specific frequencies (e.g., 40 Hz) enhances cognitive function and ameliorates neuropathological changes in experimental models[10-12]. Non-invasive approaches such as whole-body vibration or transcranial ultrasound stimulation have demonstrated neuroprotective and cognitive benefits in both animals and humans[13,14]. These findings raise the possibility that targeted mechanical stimulation could restore memory function through non-pharmacological activation of neural pathways.

Therefore, we developed a specialized head-mounted vibrotactile stimulation system (HVSS) in mice to deliver controlled vibration to the brain. Using a scopolamine hydrobromide (SCP)- induced model of reversible cholinergic dysfunction, which pharmacologically mimics acetylcholine loss-related cognitive impairment, we investigated whether HVSS could ameliorate cognitive deficits and improve cholinergic and antioxidant function. Behavioral outcomes (measured using passive avoidance and Morris water maze tests), cholinergic function, oxidative stress markers, hippocampal histopathology, and memory-related signaling gene expression were analyzed.

Materials and Methods

Animals and Treatments

Male SPF/VAF inbred C57BL/6NCrlOri mice (6-weeks old; 19–22g) were purchased from OrientBio (Seongnam, Korea). Mice were housed five per cage under controlled environmental conditions (20–25°C, 40–45% humidity, 12 h light/dark cycle) with *ad libitum* access to standard rodent chow (Cat. No. 38057; Purinafeed, Seongnam, Korea) and water. After 1 week of acclimatization, mice were randomly assigned to five groups (n= 20/group), matched by body weight (mean, 20.60 ± 0.93 g; range, 18.80–23.00 g) and baseline behavior.

Memory impairment was induced via intraperitoneal administration of scopolamine hydrobromide (1 mg/kg; Sigma-Aldrich, St. Louis, MO, USA) dissolved in 0.9% sterile saline (0.1 mg/mL), administered 1 h after the 7th, 14th, and 28th day of stimulation[15-19]. Control mice received equal volumes of saline to account for injection-related stress.

Vibrotactile stimulation was delivered using a custom-designed head-mounted vibrotactile stimulation system (HVSS), developed in collaboration with AriBio (Seongnam, Korea), combined with an acrylic cylindrical restrainer (ø35×110 mm; JD-R-05A, Jeung Do Bio & Plant Co., Ltd., Seoul, Korea). Mice were subjected to 20, 40, and 80 Hz vibratory stimulation at a fixed voltage of 2.9 V (10 min/day, for 28 consecutive days). To account for potential confounding effects related to restraint-induced stress and device attachment, sham group animals were subjected to identical handling, restraint duration, and device placement without active stimulation. The head-mounted device was designed to minimize contact-related discomfort. In addition, to ensure physiological adaptation to the experimental conditions, all animals were fasted for at least 18 h (with free access to water) prior to the first stimulation, thereby minimizing stress and inter-individual variability attributable to food restriction during the procedure. All procedures were approved by the Institutional Animal Care and Use Committee of Daegu Haany University (Approval No. DHU2023-049) and conducted in accordance with national guidelines for the care and use of laboratory animals.

Monitoring of Body Weight Changes

Body weight was recorded using an automatic electronic balance (XB320M, Precisa Instrument, Dietikon, Switzerland) at baseline (one day before the first stimulation), on the first day of vibrotactile stimulation, and on days 1, 6, 13, 20, 27, and 28 of the experimental periods. To minimize inter-individual variability, all animals were fasted for at least 18 h (with free access to water) prior to the first stimulation. To evaluate physiological changes and potential systemic toxicity, body weight gain over the 28-day experimental period was calculated as follows:

Body weight gain (g) = Body weight on day 28 - Body weight on day 0

Passive Avoidance Task for Memory Assessment

The step-through passive avoidance task was performed using a two-compartment apparatus (Cat No. 7550, Ugo Basile, Selangor, Malaysia) with light/noise and electric

shock compartments separated by a guillotine door. The training trial was conducted 30 min after SCP injection. Each mouse was placed in the illuminated chamber. After 15 s, the light and noise stimuli were activated, prompting the mouse to enter the adjacent dark chamber, upon which the door was closed, and a foot shock (3.0 mA, 3 s) was delivered through the grid floor. Mice that did not enter the dark chamber within 120 s were excluded from further tests. The retention trial was conducted 24 h later under identical conditions, except that no shock was administered. Step-through latency (maximum cut-off time: 300 s) was recorded to assess memory retention. The passive avoidance test was performed on day 28, 24 h after the final SCP injection and vibrotactile stimulation.

Morris Water Maze for Spatial Memory Evaluation

Spatial learning and memory were evaluated using the Morris water maze, as previously described with modifications[15,20-22]. The apparatus consisted of a circular pool (diameter: 100 cm, height: 37 cm) filled with water maintained at 22°C to a depth of 27 cm. A submerged escape platform (diameter: 10 cm) was placed in one of the four quadrants, and the location remained fixed throughout the training and test phases. The training trial was conducted 30 min after SCP injection. Mice were placed into the pool facing the well at one of the three non-target quadrants, and allowed to search for the platform for up to 150 s. If the mouse failed to locate the platform, it was guided to it and allowed to remain there for 10 s. A retention trial was performed 24 h after the final training session under the same conditions, with the platform maintained in its original location, and escape latency was recorded to assess memory retention. The time taken for the mouse to escape from the water onto the platform was measured as the escape latency time, with 300 s as the maximum cut-off time. Behavior tracking was performed using a video tracking system (Smart Junior, PanLab, Barcelona, Spain). This task test was conducted on day 28 of the experimental schedule, using a different cohort of animals from those used in the passive avoidance task.

Analysis of Hippocampal ACh Levels and AChE Activity

To evaluate the effects of vibrotactile stimulation on cholinergic function, hippocampal ACh

content and AChE activity were assessed using a fluorometric assay. On day 28, immediately after the passive avoidance test, mice were sacrificed under inhalation anesthesia, and the hippocampus was rapidly dissected on ice. Tissue samples were snap-frozen and stored at -150°C until analysis. Hippocampal tissue was homogenized in ice-cold 0.01 M Tris-HCl buffer (pH 7.4) using a bead beater (Taco™Pre, GeneResearch Biotechnology Corp., Taichung, Taiwan) and an ultrasonic cell disruptor (KS-750, Madell Technology Corp., Ontario, CA, USA). Homogenates were centrifuged at 12,000 g for 15 min at 4°C, and the supernatant was collected for analysis[15,17,23]. ACh levels and AChE activity were quantified using the Amplex Red Acetylcholine/Acetylcholinesterase Assay Kit (Cat No. A12217, Invitrogen, Grand Island, NY, USA), following the manufacturer's protocol. The assay reaction mixture contained 400 μM Amplex Red reagent, 2 U/mL horseradish peroxidase, and 0.2 U/mL choline oxidase. Reaction was initiated by the addition of 100 μM ACh and 100 U/mL AChE. Fluorescence intensity was measured using a microplate reader (excitation wavelength of 560 nm; emission wavelength of 590 nm). Background fluorescence was subtracted using negative controls.

Hippocampal Gene Expression Analysis by qRT-PCR

To elucidate the molecular mechanisms underlying the anti-amnesic effects of vibrotactile stimulation, the mRNA expression of ChAT and memory-associated signaling genes was analyzed in the hippocampus using quantitative real-time PCR (qRT-PCR)[15-17]. Total RNA was extracted from hippocampal samples collected immediately after the passive avoidance test using TRIzol reagent (Invitrogen, Carlsbad, CA, USA). To remove contaminating DNA, samples were treated with recombinant DNase I (DNA-free; DNA-free DNA Removal kit; Cat No. AM1906, Thermo Fisher Scientific Inc., Rockford, IL, USA). Reverse transcription was performed using the High-Capacity cDNA Reverse Transcription Kit (Cat No. 4368813, Thermo Fisher Scientific Inc.) according to the manufacturer's instructions. qRT-PCR was conducted using the CFX96™ Real-Time System (Bio-Rad, Hercules, CA, USA) was used for the analysis. Thermal cycling was performed under the following conditions: 50°C for 2 min (activation); 95°C for 10 min (pre-soak); 95°C for 15 s (denaturation); 60°C for 1 min (annealing); 95°C for 15 s, 60°C for 15 s, and 95°C for 15 s

(melting curve). Gene expression levels were normalized to Actb and calculated using the $2^{-\Delta\Delta Ct}$ method[24,25]. All qPCR primer pairs (Table 1) were obtained from OriGene Technologies (Rockville, MD, USA).

Histopathological Analysis of the Hippocampus

Hippocampal tissue was collected after completion of behavioral testing and fixed in 10% neutral buffered formalin for 24 h. Brains were processed using an automated tissue processor (Shandon Citadel 2000, Thermo Scientific, Waltham, MA, USA) and embedded in paraffin. Coronal sections (3–4 µm) containing the hippocampal formation were cut using a microtome (RM2255, Leica Biosystems, Nussloch, Germany). Cresyl violet staining was used to evaluate hippocampal cytoarchitecture, including layer thickness and overall cellular organization. Histological analysis was performed in a blinded manner using a light microscope (Eclipse 80i, Nikon, Tokyo, Japan) equipped with a digital camera system (ProgRes™ C5, Jenoptik Optical Systems GmbH, Jena, Germany) and image analysis software (*i*Solution FL ver 9.1, IMT *i*-solution Inc., Bernaby, BC, Canada). Quantitative analysis included measurement of mean CA1-CA3 thicknesses and the density of cells in the dentate gyrus (DG; cells/mm^2).

Immunohistochemistry

Immunoreactivities for cleaved caspase-3, an apoptosis marker[26,27], and c-Fos, an indirect marker of neuronal activity[17,28,29], were investigated using the avidin-biotin-peroxidase complex (ABC) and a peroxidase substrate kit (Vector Labs, Burlingame, CA, USA) and the appropriate primary antibodies (Table 2). Briefly, endogenous peroxidase activity was quenched with 0.3% H_2O_2 in methanol for 30 min, and non-specific immunoglobulin binding was blocked using normal horse serum blocking solution for 1 h in a humidity chamber after citrate buffer antigen (epitope) retrieval pretreatment of the prepared unstained sections. Sections were incubated with primary antibodies overnight at 4°C in a humidity chamber and then with biotinylated universal secondary antibodies and ABC reagents for 1 h at room temperature. Finally, sections were reacted with the peroxidase kit substrate for 3 min at room temperature. All sections were rinsed in 0.01 M phosphate-

buffered saline (PBS) thrice between each step, and finally counter-stained with Mayer's hematoxylin (Cat No. ab220365; Abcam, Cambridge, UK). Cells with >20% of immunoreactivity for cleaved caspase-3 and c-Fos were regarded as positive. The numbers of immunolabeled pyramidal cells in the DG regions were counted using a computer-based automated image analyzer as previously described[17,26,28,29]. One tissue section per animal was obtained from each of the 10 mice per group. Each section was analyzed at five independent regions of interest, and the mean value was used for subsequent statistical analysis.

Evaluation of Antioxidant Enzyme Activities in the Cerebral Cortex

On day 28, the mice were decapitated immediately following the Morris water maze test under inhalation anesthesia. The cerebral cortex was removed, and malondialdehyde (MDA) and glutathione (GSH) levels and ChAT and superoxide dismutase (SOD) enzyme activities were assessed to evaluate the cerebral antioxidant defense systems. The separated cerebral cortex was weighed and homogenized in a buffer consisting of 10 mM sucrose, 10 mM Tris–HCl, and 0.1 M EDTA (pH 7.4) and then centrifuged at 12,000 g for 15 min[30]. Lipid peroxidation was measured by determining MDA levels using the thiobarbituric acid reactive substances (TBARS) assay. Absorbance was read at 525 nm using a UV/VIS spectrophotometer (OPTIZEN POP, Mecasys, Daejeon, Korea), and results were expressed as nM MDA per gram of tissue. Total protein levels were measured using bovine serum albumin (Invitrogen) as the internal standard. To measure GSH levels, prepared homogenates were mixed with 0.1 mL of 25% trichloroacetic acid (Merck, San Francisco, CA, USA) and centrifuged at 4,200 rpm for 40 min at 4ºC. GSH levels were measured (at absorbance 412 nm) using 2-nitrobenzoic acid (Sigma-Aldrich, St. Louise, MO, USA) as nM/mg protein. Decomposition of H_2O_2 in the presence of CAT was followed at 240 nm. ChAT activity was defined as the amount of enzyme required to decompose 1 nM of H_2O_2 per minute at 25°C and pH 7.8. Results were expressed as U/mg protein. Measurements of SOD activity were made according to Sun et al.[31]. Specifically, these measurements were based on the generation of superoxide radicals produced by xanthine and xanthine oxidase, which react with nitrotetrazolium blue to form formazan dye. SOD activity was

then measured at 560 nm by the degree of inhibition of this reaction, and expressed as U/mg protein. One unit of SOD enzymatic activity is equal to the amount of enzyme that diminishes the initial absorbance of nitroblue tetrazolium by 50% in 1 min.

Histopathological Assessments of Brain and Adrenal Gland

On day 28, immediately after completion of the Morris water maze test, mice were anesthetized with isoflurane (2–3% in 70% N_2O and 28.5% O_2) and sacrificed. The whole brain (excluding the olfactory bulb) and adrenal glands were carefully dissected and subjected to gross morphological inspection.

For histopathology evaluation, the cerebrum (including hippocampal regions) and adrenal glands were fixed in 10% neutral buffered formalin for 24 h, processed using an automated tissue processor, embedded in paraffin, and sectioned at 3–4 μm thickness. The adrenal gland sections were stained with hematoxylin and eosin (H&E) and cresyl violet for histopathological observation. Histological profiles were observed under a light microscope equipped with a digital imaging system and analyzed using a computer-assisted image analyzer (iSolution FL ver.9.1, IMT i-solution Inc.).

For corticosterone analysis, blood samples (~0.8 mL) were collected from the vena cava under anesthesia, and serum was obtained by centrifugation (3,000 rpm, 10 min, 4°C). Serum corticosterone concentrations were measured using a commercial ELISA kit (LSBio LS-F67102, Seattle, WA, USA) according to the manufacturer's protocol, with duplicate readings taken for each sample.

Statistical Analysis

All data are presented as mean ± standard deviation (SD). Statistical analyses were performed using GraphPad Prism (version 10.4.2, GraphPad Software, SanDiego, CA, USA). Group comparisons were conducted using one-way analysis of variance (ANOVA) followed by Tukey's post hoc test for multiple comparisons. Differences were considered statistically significant at $p < 0.05$ (*), < 0.01 (**), < 0.001 (***), and < 0.0001 (****). MWM training trial data were presented descriptively to illustrate learning progression across groups and

were excluded from formal statistical analysis. Percent changes in the vibrotactile stimulation groups as compared with the SCP control group were also calculated to assess the efficacy of vibrotactile stimulations, and percent changes between the intact vehicle and SCP control groups were calculated to assess amnesia induction status using the following equations:

Percentage changes as compared with intact vehicle controls (%)

= ((Data of SCP control – data of vehicle control)/data of vehicle control) × 100

Percentage changes as compared with SCP control (%)

= ((Data of vibrotactile stimulated groups – data of SCP control)/data of SCP control) × 100

Results

Head-mounted vibrotactile stimulation improves scopolamine-induced memory impairments in mice

To investigate whether HVSS improves SCP-induced cognitive impairment, mice were treated with SCP (1 mg/kg, i.p.) and exposed to 20, 40, or 80 Hz vibration for 10 min daily over a 28-day period. Figure 1A shows the stimulation setup and vibration frequencies applied to the skull, Figure 1B presents the actual HVSS device, and Figure 1C depicts the 28-day experimental schedule.

In the passive avoidance test, SCP-treated mice exhibited a markedly shorter step-through latency (55.6 ± 10.4 s) compared to vehicle-treated controls (191.7 ± 20.3 s), indicating impaired memory retention (Fig. 1D). Vibrotactile stimulation at 40 and 80 Hz significantly increased latency to 101.3 ± 15.6 s and 100.1 ± 12.7 s, whereas 20 Hz stimulation produced only a modest and non-significant change. Mice treated with 40 or 80 Hz HVSS showed a comparable level of improvement, with no significant difference between these two frequencies.

In the Morris water maze task, SCP-treated mice exhibited significantly prolonged escape latency (144.0 ± 12.2 s) compared to vehicle controls (38.8 ± 10.3 s) ($p < 0.0001$), confirming impaired spatial learning. Vibrotactile stimulation at 40 and 80 Hz significantly reduced escape latency to 74.5 ± 13.7 s and 72.7 ± 14.1 s, respectively, while 20 Hz stimulation again had no significant effect (Fig. 1E).

These findings support that higher frequency vibrotactile stimulation effectively ameliorates SCP-induced cognitive deficits.

HVSS modulates hippocampal cholinergic function in SCP-induced mice

We next assessed whether HVSS could influence the hippocampal cholinergic system by measuring ChAT transcript levels (encoded by *CHAT*), ACh contents, and AChE activities. As shown in Figure 2A, SCP administration markedly reduced ChAT mRNA expression (0.31 ± 0.07-fold) compared with vehicle controls (1.00 ± 0.08-fold). Stimulation at 20 Hz produced no detectable change relative to SCP controls, whereas both 40 and 80 Hz stimulation significantly restored ChAT levels to 0.58 ± 0.06 and 0.58 ± 0.07-fold. The effects of 40 and 80 Hz were comparable, showing no significant difference between the two groups. Consistent with the gene expression data, hippocampal ACh contents were significantly decreased in SCP controls (25.4 ± 7.8%, $p < 0.0001$) relative to vehicle controls. Vibrotactile stimulation at 40 and 80 Hz markedly elevated ACh concentrations to 47.9 ± 5.8% and 48.0 ± 6.3%, respectively, whereas 20 Hz stimulation did not alter the SCP-induced reduction. Again, the extent of recovery at 40 and 80 Hz was similar (Fig. 2B). In parallel, hippocampal AChE activity was significantly increased by SCP treatment (256.2 ± 34.8%) compared with vehicle controls. This elevation was not affected by 20 Hz stimulation, but both 40 and 80 Hz stimulation significantly suppressed AChE activity (171.9 ± 20.9% and 171.0 ± 15.7%, $p < 0.0001$). The two higher-frequency groups did not differ significantly from each other (Fig. 2C).

HVSS attenuates oxidative stress and restores antioxidant defense in the cerebral cortex

To evaluate the cerebral antioxidant defense system, the level of oxidative stress-related

markers was analyzed in the cerebral cortex[17,32,33]. As shown in Figure 3A, SCP administration markedly increased MDA levels (5.06 ± 0.94 nM/mg protein) compared with vehicle (1.78 ± 0.42), indicating enhanced lipid peroxidation. Vibrotactile stimulation at 40 Hz and 80 Hz significantly reduced MDA to 3.21 ± 0.42 and 3.28 ± 0.51, whereas 20 Hz stimulation produced no meaningful change. As shown in Figure 3B, GSH content was significantly depleted in SCP-treated mice (1.96 ± 0.30 nM/mg) relative to vehicle (8.59 ± 0.75) but was effectively restored by high-frequency HVSS (4.17 ± 0.61 at 40 Hz; 4.24 ± 0.81 at 80 Hz). Similarly, Figure 3C shows that CAT activity decreased to 10.67 ± 2.24 U/mg in SCP treatment (49.91 ± 10.25 in vehicle) and was increased to approximately 21.8 ± 3.5 with 40 Hz and 80 Hz stimulation. As shown in Figure 3D, SOD activity was reduced to 5.70 ± 1.52 U/mg compared with vehicle levels (32.78 ± 11.91) and restored to 13.9 ± 2.8 and 13.8 ± 3.8 following 40 Hz and 80 Hz stimulation, respectively. These alterations were effectively counteracted by vibrotactile stimulation at 40 and 80 Hz, which significantly suppressed the elevation of MDA and restored GSH levels as well as CAT and SOD activities relative to SCP controls. In contrast, stimulation at 20 Hz failed to produce significant changes in any of these parameters compared with SCP controls. Notably, the extent of recovery was comparable between the 40 and 80 Hz groups, with no significant differences detected.

HVSS preserves hippocampal structure and alleviates neuronal dysfunction

Histopathological alterations in the hippocampus were evaluated using cresyl violet staining and immunostaining of cleaved caspase-3 and c-Fos. As shown in Figure 4A, SCP administration caused significant reductions in CA1-CA3 layer thickness (20.2 ± 7.1%) and overall neuronal density (34.7 ± 8.6%) compared with intact controls. High-frequency HVSS (40 and 80 Hz) markedly reversed these structural deficits, restoring thickness by 15.1 ± 6.5% and 14,3 ± 5.9% and increasing viable cell counts by 34.5 ± 6.7% and 32.5 ± 6.3%, whereas 20 Hz stimulation produced no significant change.

AS shown in Figure 4B, cleaved caspase-3 pyramidal cells (red, arrows) markedly increased following SCP treatment (404 ± 24.6%,) indicating pronounced apoptosis, which was

significantly suppressed by 40 Hz and 80 Hz HVSS (52.8 ± 6.9% and 53.2 ± 6.3% reductions, respectively).

Conversely, neuronal activation assessed by c-Fos immunoreactivity (red, arrows) decreased by 88.6 ± 7.5% in SCP-treated mice but was robustly recovered by 40 Hz and 80 Hz HVSS (446.7 ± 24.3% and 440.0 ± 22.8% increases, respectively), while 20 Hz stimulation had no effect (Fig. 4C).

Collectively, these results demonstrate that high-frequency HVSS (40-80 Hz) mitigates SCP-induced hippocampal degeneration by preserving structural integrity, reducing apoptosis, and reactivating neuronal populations associated with cognitive function.

HVSS enhances hippocampal expression of memory-related signaling genes

To explore the molecular basis of HVSS-mediated neuroprotection, hippocampal mRNA levels of memory-related genes, including *BDNF*, *PI3K*, *AKT*, *ERK1/2*, *CREB*, and *CAMK4*, were quantified by qRT-PCR. In Figure 5A, SCP administration markedly reduced *BDNF* mRNA levels to 0.31 ± 0.05-fold of vehicle levels (1.00 ± 0.06), while HVSS at 40 and 80 Hz significantly elevated BDNF expression to 0.49 ± 0.06 and 0.49 ± 0.07-fold, respectively. As shown in Figure 5B, *PI3K* transcripts were decreased to 0.30 ± 0.06-fold in SCP-treated mice (1.01 ± 0.08 in vehicle) but significantly increased to 0.52 ± 0.07-fold under both 40 and 80 Hz stimulation. Similarly, Figure 5C demonstrates that Akt expression encoded by *AKT* declined to 0.30 ± 0.07-fold in SCP-treated mice and was recovered to 0.50 ± 0.08-fold and 0.49 ± 0.07-fold following high-frequency HVSS. SCP exposure also reduced *ERK1* levels (0.25 ± 0.07-fold), which recovered to 0.44 ± 0.05 and 0.44 ± 0.06-fold in 40 and 80 Hz HVSS (Fig. 5D). Likewise, *ERK2* expression was suppressed to 0.21 ± 0.08-fold and increased to 0.42 ± 0.04-fold under 40 and 80 Hz stimulation (Fig. 5E). In Figure 5F, *CREB* mRNA decreased to 0.30 ± 0.05-fold of vehicle (1.00 ± 0.09) and recovered to 0.52 ± 0.07-fold and 0.52 ± 0.10-fold with 40 and 80 Hz HVSS. Finally, CaMK IV encoded by *CAMK4* expression declined to 0.27 ± 0.07-fold and was increased to 0.51 ± 0.10-fold and 0.51 ± 0.08-fold following 40 and 80 Hz stimulation. No significant differences were observed between the 40 and 80 Hz groups.

Together, these findings indicate that HVSS at 40 and 80 Hz effectively counteract SCP-induced suppression of hippocampal memory-related signaling pathways, whereas low-frequency stimulation at 20 Hz remains ineffective. In addition, physiological and endocrine safety were assessed to exclude systemic side effects of HVSS. No significant differences were observed in body weight (Supplementary Fig. S1), brain morphology (Supplementary Fig. S2), adrenal gross morphology (Supplementary Fig. S3), adrenal glands histopathology (Supplementary Fig. S4), or serum corticosterone levels (Supplementary Fig. S5), suggesting that HVSS did not induce stress-related or endocrine alterations.

Discussion

Transcranial vibrotactile stimulation delivered via HVSS ameliorated SCP–induced cholinergic dysfunction-related memory impairment in mice in a frequency-dependent manner. Stimulation at 40 and 80 Hz improved both passive avoidance and spatial memory performance (Fig. 1), accompanied by recovery of hippocampal cholinergic function (Fig. 2) and attenuation of oxidative stress with reduced MDA and recovered GSH, SOD, and CAT activities (Fig. 3). HVSS also preserved hippocampal morphology and enhanced neuronal activation (Fig. 4), while upregulating memory-related genes such as *BDNF*, *PI3K*, *AKT*, *ERK1/2*, *CREB*, and *CAMK4* (Fig. 5). Together, these results indicate that high-frequency HVSS improves cognitive performance through coordinated regulation of cholinergic signaling and oxidative balance. A limitation of this study is that mechanistic interpretations are based on mRNA expression data. Future studies incorporating protein-level analyses, including phosphorylation states (e.g., *p-AKT*, *p-CREB*) and total protein quantification (e.g., *BDNF*), are warranted to fully substantiate the proposed signaling mechanisms."

These findings are consistent with previous reports that sensory or mechanical neuromodulation, such as vibration-, ultrasound, or light-based stimulation, can ameliorate cholinergic dysfunction and cognitive decline in neurodegenerative models[34-37]. However,

most prior approaches depended on systemic or sensory-entrainment effects rather than direct mechanical transmission to the brain, limiting their ability to precisely target neural circuits. In contrast, HVSS delivers frequency-specific mechanical oscillations directly through the skull, providing localized tactile-mechanical modulation of cortical and hippocampal activity. This distinction highlights HVSS as a mechanically direct, non-pharmacological strategy capable of enhancing cognitive function and neural homeostasis through physical coupling to brain tissue.

The antioxidant and molecular changes observed here align with prior studies linking SCP and AD-related pathology to oxidative imbalance[32,33]. HVSS significantly reduced lipid peroxidation and boosted endogenous antioxidant capacity, changes that likely contributed to the reduced apoptosis and improved neuronal activation observed in hippocampal subfields (Figs. 3 and 4). In parallel, partial amelioration of *BDNF*, *PI3K*, *AKT*, *ERK*, *CREB*, and *CAMK4* expression levels (Fig. 5) suggests that attenuation of oxidative stress promotes activation of antioxidant-sensitive cascades involved in synaptic plasticity and memory formation. These findings imply that HVSS exerts neuroprotective effects not only through attenuation of oxidative stress but also by initiating mechanotransductive signaling processes sensitive to vibration frequency.

Although cerebral blood flow was not directly assessed, previous imaging studies suggest that vibrotactile stimulation can transiently enhance regional perfusion through mechanical-vascular coupling[38,39]. Such hemodynamic facilitation could indirectly support the metabolic and cholinergic improvements observed here, warranting further investigation into vascular responses to HVSS.

The frequency specificity of HVSS is an important feature. Both 40 and 80 Hz stimulation were comparably effective, whereas 20 Hz was ineffective, suggesting that vibrotactile inputs engage mechanotransductive pathways in neurons and glia only within specific frequency ranges. This frequency-dependent response is unlikely to reflect a nonspecific dose-response relationship, but rather may arise from intrinsic differences in neural circuit resonance and oscillatory entrainment mechanisms. Notably, 40 Hz corresponds to the

intrinsic resonance frequency of fast-spiking parvalbumin-positive (FS-PV) interneuron network, which play a central role in generating gamma oscillations through tightly coupled excitatory-inhibitory (E-I) interactions[40,41]. In contrast, 20 Hz falls within the beta frequency range, which preferentially engages sensorimotor circuits rather than the gamma-generating networks associated with cognition, glial modulation, and synaptic plasticity[42]. Consistent with this distinction, previous studies have demonstrated that selective activation of FS-PV interneurons at 40 Hz, but not at other frequencies including 20 Hz, induces amyoid-beta clearance and enhances microglial phagocytic activity in Alzheimer's disease models[43], supporting the idea that gamma-frequency stimulation represents a privileged neurobiological window that cannot be effectively accessed by lower-frequency inputs. Although mechanotransductive pathways were not directly examined in this study, our previous work demonstrated that 40 Hz vibrotactile stimulation suppressed amyloid-beta-induced neurotoxicity and restored cellular homeostasis in SH-SY5Y, BV2 cells, and pericytes[44], supporting the possibility that similar mechanically induced signaling mechanisms contribute to the hippocampal and behavioral protective effects observed in the present study. Among these, 40 Hz stimulation has been most extensively characterized and is known to entrain gamma-band oscillations associated with attention, working memory, and synaptic plasticity[34,37,44]. Previous studies have shown that 40 Hz sensory or mechanical stimulation can upregulate BDNF-related signaling pathways (including PI3K/Akt, ERK, and CREB), enhance neuronal synchrony, and reduce amyloid or oxidative pathology in experimental models[37,44]. Consistent with these findings, 40 Hz HVSS in the present study improved cognitive performance and activated memory-related molecular pathways in the hippocampus, indicating that this frequency may optimally engage neuroplastic and antioxidant mechanisms. The relationship between 40 and 80 Hz is mechanistically distinct from the contrast between 40 and 20 Hz. As the second harmonic of 40 Hz, 80 Hz stimulation may engage gamma oscillatory networks through subharmonic entrainment, whereby neural systems driven at 80 Hz can generate coherent responses at 40 Hz due to the intrinsic tendency of gamma oscillators to phase-lock at harmonic rations[40,45]. This harmonic organization is consistent with

observations that thalamocortical circuits exhibit resonance peaks at multiple integer-related frequencies, including 40 and 80 Hz[45]. Nevertheless, 40 Hz and 80 Hz are not functionally identical. Previous studies have shown that 40 Hz stimulation preferentially enhances gamma power and cognitive performance through astrocyte-interneuron interactions, whereas 80 Hz stimulation can modulate neural activity via distinct high-gamma mechanisms[46,47], indicating that these frequencies engage overlapping but non-identical neural substrates.

Moreover, 80 Hz stimulation has demonstrated meaningful neurophysiological and behavioral benefits across multiple biological levels and stimulation modalities. In humans, 80 Hz tACS enhanced visuospatial working-memory performance and increased motor cortical excitability[48,49]. In patients with Parkinson's disease, subthalamic DBS at 80 Hz alleviated levodopa-induced dyskinesia and transiently improved gait function[50,51]. In a Parkinson's disease mouse model, chronic 80 Hz auditory or visual stimulation attenuated α-synuclein pathology and ameliorated both motor and non-motor deficits[52]. At the cellular-circuit level, optogenetic activation of microglia at 80 Hz increased neuronal excitability in neighboring circuits[53]. Together, these findings indicate that the effective frequency range within the gamma sub-band extends beyond 40 Hz and that 80 Hz stimulation can also engage biologically relevant pathways across species and modalities.

HVSS also demonstrated excellent safety and tolerability, as no adverse changes were detected in body weight, brain or adrenal morphology, or serum corticosterone. These findings support the feasibility of repeated, non-invasive HVSS for chronic use in preclinical models. While pharmacological AChE inhibition remains a mainstay symptomatic therapy for mild AD[1], its efficacy is limited by adverse effects such as hepatotoxicity[4,5]. The recently approved anti-amyloid monoclonal antibodies, the first disease-modifying treatment, show only moderate efficacy and carry high costs as well as risks of adverse events such as Amyloid-Related Imaging Abnormalities (ARIA)[6,7,54]. In contrast, HVSS provides a complementary, low-risk therapeutic avenue capable of achieving similar cognitive benefits without pharmacological burden, while concurrently engaging antioxidant and neuroprotective mechanisms. While the precise mechanism by which HVSS-induced

mechanical stimulation affects the hippocampus has not yet been fully elucidated in this study, we propose the following mechanistic hypothesis based on existing literature. First, low-frequency mechanical vibrations are known to propagate through the skull via bone conduction and can be transmitted into brain tissue as mechanical waves. Due to their long wavelength, such vibrations are capable of penetrating deeper brain structures and may be distributed through cerebrospinal fluid (CSF) and interstitial fluid pathways[55-57]. In addition, mechanical vibrations of the skull have been reported to influence CSF dynamics and facilitate fluid movement within the brain[58,59]. Second, these mechanical inputs can be converted into biological signals through mechanotransduction processes involving neurons and glial cells. The brain is a highly mechanosensitive organ, and mechanical cues are sensed through mechanosensitive ion channels (e.g., Piezo1), which convert physical forces into intracellular biochemical signaling cascades[46,47]. Such processes are known to regulate neuronal activity, glial responses, and neurotrophic signaling pathways. Finally, the hippocampus, as a highly plastic and interconnected structure, may exhibit amplified responses to such inputs through network-level modulation. Nevertheless, further studies are needed to elucidate the underlying mechanisms, including the expression of mechanosensors and the mechanotransduction pathways activated by mechanical stimulation.

Our study still has some limitations. The mechanotransductive pathways linking vibrotactile stimulation to hippocampal signaling remain to be elucidated. In addition, the scopolamine model reflects transient cholinergic dysfunction rather than progressive neurodegeneration, and further transgenic or aging models will be necessary. Furthermore, the possibility that non-specific effects, such as changes in locomotor activity or nociceptive sensitivity, may have contributed to the behavioral outcomes cannot be fully excluded. Future studies incorporating open field tests and paw withdrawal threshold assessments are warranted to confirm that the observed improvements in step-through latency reflect genuine enhancements in memory retention rather than non-specific behavioral changes. Future studies should also evaluate the long-term durability of HVSS effects and determine whether frequency optimization can enhance outcomes across

different ages and sexes.

In summary, HVSS improved memory and hippocampal function through integrated cholinergic, antioxidant, and mechanosensitive modulation. These findings position vibrotactile neuromodulation as a promising, non-pharmacological approach for cognitive impairment and motivate further mechanistic and translational exploration in cognitive decline and memory impairment.

Conclusion

In summary, transcranial vibrotactile stimulation using HVSS effectively alleviates scopolamine-induced memory impairment in mice. Repetitive stimulation at 40 and 80 Hz improves cholinergic balance, enhances antioxidant defense, preserves hippocampal structure, and reactivates memory-related signaling pathways. These findings suggest that mechanical stimulation at specific frequencies can engage neuroprotective and cognitive networks through mechanotransductive processes. HVSS may therefore represent a safe and feasible non-pharmacological approach for preventing or ameliorating cognitive decline.

References

1 Chuong, N. N. *et al.* Anti-amnesic effect of alkaloid fraction from Lycopodiella cernua (L.) Pic. Serm. on scopolamine-induced memory impairment in mice. *Neurosci Lett* **575**, 42-46, doi:10.1016/j.neulet.2014.05.031 (2014).

2 Becker, R., Giacobini, E., Elble, R., McIlhany, M. & Sherman, K. Potential pharmacotherapy of Alzheimer disease. A comparison of various forms of physostigmine administration. *Acta Neurol Scand Suppl* **116**, 19-32, doi:10.1111/j.1600-0404.1988.tb07983.x (1988).

3 Blusztajn, J. K. & Wurtman, R. J. Choline and cholinergic neurons. *Science* **221**, 614-620, doi:10.1126/science.6867732 (1983).

4 Watkins, P. B., Zimmerman, H. J., Knapp, M. J., Gracon, S. I. & Lewis, K. W. Hepatotoxic effects of tacrine administration in patients with Alzheimer's disease. *JAMA* **271**, 992-998 (1994).

5 Park, S. M. *et al.* Tacrine, an oral acetylcholinesterase inhibitor, induced hepatic oxidative damage, which was blocked by liquiritigenin through GSK3-beta inhibition. *Biol Pharm Bull* **38**, 184-192, doi:10.1248/bpb.b14-00430 (2015).

6 Sims, J. R. *et al.* Donanemab in Early Symptomatic Alzheimer Disease: The TRAILBLAZER-ALZ 2 Randomized Clinical Trial. *JAMA* **330**, 512-527, doi:10.1001/jama.2023.13239 (2023).

7 van Dyck, C. H. *et al.* Lecanemab in Early Alzheimer's Disease. *N Engl J Med* **388**, 9-21, doi:10.1056/NEJMoa2212948 (2023).

8 Cho, H. *et al.* Neural differentiation of umbilical cord mesenchymal stem cells by sub-sonic vibration. *Life Sci* **90**, 591-599, doi:10.1016/j.lfs.2012.02.014 (2012).

9 Lee, G. Y., Kim, O. H., Kim, E. R. & Lee, H. J. Biomechanical forces in the aged brain: Relationship to AD. *Life Sci* **312**, 121237, doi:10.1016/j.lfs.2022.121237 (2023).

10 Martorell, A. J. *et al.* Multi-sensory Gamma Stimulation Ameliorates Alzheimer's-Associated Pathology and Improves Cognition. *Cell* **177**, 256-271 e222, doi:10.1016/j.cell.2019.02.014 (2019).

11 Paulson, A. L., Zhang, L., Prichard, A. M. & Singer, A. C. 40 Hz sensory stimulation enhances CA3-CA1 coordination and prospective coding during navigation in a mouse model of Alzheimer's disease. *Proc Natl Acad Sci U S A* **122**, e2419364122, doi:10.1073/pnas.2419364122 (2025).

12 Chen, X. *et al.* Unleashing the potential: 40 Hz multisensory stimulation therapy for cognitive impairment. *J Cent Nerv Syst Dis* **17**, 11795735251328029, doi:10.1177/11795735251328029 (2025).

13 Ahuja, G. *et al.* The effects of whole-body vibration therapy on immune and brain functioning: current insights in the underlying cellular and molecular mechanisms. *Front Neurol* **15**, 1422152, doi:10.3389/fneur.2024.1422152 (2024).

14 Park, M. *et al.* Effects of transcranial ultrasound stimulation pulsed at 40 Hz on Abeta plaques and brain rhythms in 5xFAD mice. *Transl Neurodegener* **10**, 48, doi:10.1186/s40035-021-00274-x (2021).

15 Hu, J. R., Chun, Y. S., Kim, J. K., Cho, I. J. & Ku, S. K. Ginseng berry aqueous extract prevents scopolamine-induced memory impairment in mice. *Exp Ther Med* **18**, 4388-4396, doi:10.3892/etm.2019.8090 (2019).

16 Lee, S. *et al.* Sulforaphane alleviates scopolamine-induced memory impairment in mice. *Pharmacol Res* **85**, 23-32, doi:10.1016/j.phrs.2014.05.003 (2014).

17 Kim, D.-W. *et al.* Anti-Amnesic Effect of Curcumin Spray Dry Powders on Scopolamine-Induced Mouse Memory Impairment. *Journal of the Korean Society of Food Science and Nutrition* **51**, 751-764, doi:10.3746/jkfn.2022.51.8.751 (2022).

18 Kim, Y. R. *et al.* Beneficial Effects of Gagam-Palmultang on Scopolamine-Induced Memory Deficits in Mice. *Evid Based Complement Alternat Med* **2018**, 3479083, doi:10.1155/2018/3479083 (2018).

19 Ryu, H. S. *et al.* Golden Oyster Mushroom Extract Ameliorates Oxidative Stress-Induced Cell Death in Neurons and Scopolamine-Induced Cholinergic System Impairment in Mice. *Mol Neurobiol*, doi:10.1007/s12035-025-05223-7 (2025).

20 Morris, R. Developments of a water-maze procedure for studying spatial learning in the rat. *J Neurosci Methods* **11**, 47-60, doi:10.1016/0165-0270(84)90007-4 (1984).

21 Hung, T. M. *et al.* Cholinesterase inhibitory and anti-amnesic activity of alkaloids from Corydalis turtschaninovii. *J Ethnopharmacol* **119**, 74-80, doi:10.1016/j.jep.2008.05.041 (2008).

22 Nam, Y. & Lee, D. Ameliorating effects of constituents from Cortex Acanthopanacis Radicis on memory impairment in mice induced by scopolamine. *J Tradit Chin Med* **34**, 57-62, doi:10.1016/s0254-6272(14)60055-8 (2014).

23 Del Rio, D., Stewart, A. J. & Pellegrini, N. A review of recent studies on malondialdehyde as toxic molecule and biological marker of oxidative stress. *Nutr Metab Cardiovasc Dis* **15**, 316-328, doi:10.1016/j.numecd.2005.05.003 (2005).

24 Schmittgen, T. D. & Livak, K. J. Analyzing real-time PCR data by the comparative C(T) method. *Nat Protoc* **3**, 1101-1108, doi:10.1038/nprot.2008.73 (2008).

25 Livak, K. J. & Schmittgen, T. D. Analysis of relative gene expression data using real-time quantitative PCR and the 2(-Delta Delta C(T)) Method. *Methods* **25**, 402-408, doi:10.1006/meth.2001.1262 (2001).

26 Kim, S. H., Chung, D. K., Lee, Y. J., Song, C. H. & Ku, S. K. Neuroprotective effects of Danggui-Jakyak-San on rat stroke model through antioxidant/antiapoptotic pathway. *J Ethnopharmacol* **188**, 123-133, doi:10.1016/j.jep.2016.04.060 (2016).

27 Xu, Q. Q. *et al.* Sodium Tanshinone IIA Sulfonate Attenuates Scopolamine-Induced Cognitive Dysfunctions via Improving Cholinergic System. *Biomed Res Int* **2016**, 9852536, doi:10.1155/2016/9852536 (2016).

28 Wirtshafter, D. Cholinergic involvement in the cortical and hippocampal Fos expression induced in the rat by placement in a novel environment. *Brain Res* **1051**, 57-65, doi:10.1016/j.brainres.2005.05.052 (2005).

29 Fast, C. D., Flesher, M. M., Nocera, N. A., Fanselow, M. S. & Blaisdell, A. P. Learning history and cholinergic modulation in the dorsal hippocampus are necessary for rats to infer the status of a hidden event. *Hippocampus* **26**, 804-815, doi:10.1002/hipo.22564 (2016).

30 Zhan, C. & Yang, J. Protective effects of isoliquiritigenin in transient middle cerebral artery occlusion-induced focal cerebral ischemia in rats. *Pharmacol Res* **53**, 303-309, doi:10.1016/j.phrs.2005.12.008 (2006).

31 Sun, Y., Oberley, L. W. & Li, Y. A simple method for clinical assay of superoxide dismutase. *Clin Chem* **34**, 497-500 (1988).

32 Mansoorali, K. P., Prakash, T., Kotresha, D., Prabhu, K. & Rama Rao, N. Cerebroprotective effect of Eclipta alba against global model of cerebral ischemia induced oxidative stress in rats. *Phytomedicine* **19**, 1108-1116, doi:10.1016/j.phymed.2012.07.004 (2012).

33 Ghumatkar, P. J., Patil, S. P., Jain, P. D., Tambe, R. M. & Sathaye, S. Nootropic, neuroprotective and neurotrophic effects of phloretin in scopolamine induced amnesia in mice. *Pharmacol Biochem Behav* **135**, 182-191, doi:10.1016/j.pbb.2015.06.005 (2015).

34 Kim, T. W. *et al.* Acceleration-Dependent Effects of Vibrotactile Gamma Stimulation on Cognitive Recovery and Cholinergic Function in a Scopolamine-Induced Neurotoxicity Mouse Model. *Biomedicines* **13**, doi:10.3390/biomedicines13082031 (2025).

35 Leinenga, G. & Gotz, J. Scanning ultrasound removes amyloid-beta and restores memory in an Alzheimer's disease mouse model. *Sci Transl Med* **7**, 278ra233, doi:10.1126/scitranslmed.aaa2512 (2015).

36 Oroszi, T. *et al.* Whole-Body Vibration Affects Hippocampal Choline Acetyltransferase and Synaptophysin Expression and Improves Spatial Memory in Young Adult Mice. *J Integr Neurosci* **23**, 173, doi:10.31083/j.jin2309173 (2024).

37 Park, S. S. *et al.* Physical exercise during exposure to 40-Hz light flicker improves cognitive functions in the 3xTg mouse model of Alzheimer's disease. *Alzheimers Res Ther* **12**, 62, doi:10.1186/s13195-020-00631-4 (2020).

38 Kong, L. *et al.* Assessment of vibration modulated regional cerebral blood flow with MRI. *Neuroimage* **269**, 119934, doi:10.1016/j.neuroimage.2023.119934 (2023).

39 Seitz, R. J. & Roland, P. E. Vibratory stimulation increases and decreases the regional cerebral blood flow and oxidative metabolism: a positron emission tomography (PET) study. *Acta Neurol Scand* **86**, 60-67, doi:10.1111/j.1600-0404.1992.tb08055.x (1992).

40 Buzsaki, G. & Wang, X. J. Mechanisms of gamma oscillations. *Annu Rev Neurosci* **35**, 203-225, doi:10.1146/annurev-neuro-062111-150444 (2012).

41 Ichim, A. M. *et al.* The gamma rhythm as a guardian of brain health. *Elife* **13**, doi:10.7554/eLife.100238 (2024).

42 Brown, P. Oscillatory nature of human basal ganglia activity: relationship to the pathophysiology of Parkinson's disease. *Mov Disord* **18**, 357-363, doi:10.1002/mds.10358 (2003).

43 Iaccarino, H. F. *et al.* Gamma frequency entrainment attenuates amyloid load and modifies microglia. *Nature* **540**, 230-235, doi:10.1038/nature20587 (2016).

44 Shin, C. H. *et al.* Vibrotactile stimulation at 40 Hz inhibits Abeta-induced changes in SH-SY5Y, BV2 cells, and pericytes. *Brain Res Bull* **220**, 111138, doi:10.1016/j.brainresbull.2024.111138 (2025).

45 Herrmann, C. S. Human EEG responses to 1-100 Hz flicker: resonance phenomena in visual cortex and their potential correlation to cognitive phenomena. *Exp Brain Res* **137**, 346-353, doi:10.1007/s002210100682 (2001).

46 Tyler, W. J. The mechanobiology of brain function. *Nat Rev Neurosci* **13**, 867-878, doi:10.1038/nrn3383 (2012).

47 Zheng, Q. *et al.* Mechanical properties of the brain: Focus on the essential role of Piezo1-mediated mechanotransduction in the CNS. *Brain Behav* **13**, e3136,

doi:10.1002/brb3.3136 (2023).
48 Park, J., Lee, C., Lee, S. & Im, C. H. 80 Hz but not 40 Hz, transcranial alternating current stimulation of 80 Hz over right intraparietal sulcus increases visuospatial working memory capacity. *Sci Rep* **12**, 13762, doi:10.1038/s41598-022-17965-8 (2022).
49 Rostami, M. *et al.* Determining the effects of transcranial alternating current stimulation on corticomotor excitability and motor performance: A sham-controlled comparison of four frequencies. *Neuroscience* **568**, 12-26, doi:10.1016/j.neuroscience.2025.01.016 (2025).
50 Merola, A. *et al.* 80 Hz versus 130 Hz subthalamic nucleus deep brain stimulation: effects on involuntary movements. *Parkinsonism Relat Disord* **19**, 453-456, doi:10.1016/j.parkreldis.2013.01.006 (2013).
51 Ricchi, V. *et al.* Transient effects of 80 Hz stimulation on gait in STN DBS treated PD patients: a 15 months follow-up study. *Brain Stimul* **5**, 388-392, doi:10.1016/j.brs.2011.07.001 (2012).
52 Liu, Y. *et al.* Non-invasive auditory and visual stimulation attenuates alpha-Synuclein deposition and improves motor and non-motor symptoms in PD mice. *Exp Neurol* **364**, 114396, doi:10.1016/j.expneurol.2023.114396 (2023).
53 Nagarajan, N. & Capecchi, M. R. Optogenetic stimulation of mouse Hoxb8 microglia in specific regions of the brain induces anxiety, grooming, or both. *Mol Psychiatry* **29**, 1726-1740, doi:10.1038/s41380-023-02019-w (2024).
54 Greenberg, S. M., Bax, F. & van Veluw, S. J. Amyloid-related imaging abnormalities: manifestations, metrics and mechanisms. *Nat Rev Neurol* **21**, 193-203, doi:10.1038/s41582-024-01053-8 (2025).
55 Sohmer, H., Freeman, S., Geal-Dor, M., Adelman, C. & Savion, I. Bone conduction experiments in humans - a fluid pathway from bone to ear. *Hear Res* **146**, 81-88, doi:10.1016/s0378-5955(00)00099-x (2000).
56 Lee, J. *et al.* Contralateral bone conducted sound wave propagation on the skull bones in fresh frozen cadaver. *Sci Rep* **13**, 7479, doi:10.1038/s41598-023-32307-y (2023).
57 Freeman, S., Sichel, J. Y. & Sohmer, H. Bone conduction experiments in animals - evidence for a non-osseous mechanism. *Hear Res* **146**, 72-80, doi:10.1016/s0378-5955(00)00098-8 (2000).
58 Jindrak, K. F. & Jindrak, H. Mechanical effect of vocalization on human brain and meninges. *Med Hypotheses* **25**, 17-20, doi:10.1016/0306-9877(88)90040-0 (1988).
59 Kong, L. *et al.* Transcranial vibration stimulation at 40 Hz induced neural activity and promoted the coupling of global brain activity and cerebrospinal fluid flow. *Neuroimage* **308**, 121074, doi:10.1016/j.neuroimage.2025.121074 (2025).

Acknowledgments

We express our sincere gratitude to all researchers and technical staff who contributed to this study. We also thank the personnel involved in animal care and data collection for their dedicated efforts throughout the experimental procedures. ESC was supported by the Chung-Ang University Graduate Research Scholarship in 2024.

Funding

The authors received no specific funding for this work.

Ethics declarations

Ethic Approval

All animal care and experimental procedures have been approved by the Institutional Animal Care and Use Committee of Daegu Haany University (Approval No. DHU2023-049).

Clinical Trials

Not applicable

Competing Interests

The authors declare no competing interests.

Author Contributions

O-HK: Investigation, Data curation, Validation, Writing—original draft, Writing—review and editing.

C-HS: Conceptualization, Methodology, Validation, Writing—original draft, Writing—review and editing.

M-WC: Methodology, Resources.

J-YH: Resources, Project administration.

JJC: Conceptualization, Supervision.

D-KS: Conceptualization, Data curation, Validation, Writing—review and editing.

J-YC: Methodology, Resources.

ESC: Resources, Writing—review and editing.

HJL: Conceptualization, Supervision, Writing—review and editing.

S-KK: Conceptualization, Methodology, Data curation, Formal analysis, Writing—original draft

Figure legends

Figure 1. Experimental design and behavioral performance following HVSS. (A) Schematic illustration of vibration applied to the mouse head. (B) Photograph of the head-mounted vibrotactile stimulation system. (C) Experimental schedule for SCP administration, HVSS treatment, and behavioral test. (D) Step-through latency in the passive avoidance test (n = 10, ****p < 0.0001). (E) Escape latency in the Morris water maze test (n = 10, ****p < 0.0001).

Figure 2. HVSS enhances hippocampal cholinergic function in mice with SCP-induced dysfunction. (A) Relative transcript levels of choline acetyltransferase (*CHAT*) measured by qRT-PCR (n = 10, ****p < 0.0001). (B) Hippocampal acetylcholine (ACh) contents determined by assay kit (n = 10, ****p < 0.0001). (C) Hippocampal acetylcholinesterase (AChE) activity measured using an enzymatic activity assay (n = 10, ****p < 0.0001).

Figure 3. HVSS alleviates oxidative stress and enhances antioxidant defense in the cerebral cortex. (A) Cortical malondialdehyde (MDA) levels as an indicator of lipid peroxidation (n = 10, ****p < 0.0001). (B) Glutathione (GSH) contents as an endogenous antioxidant (n = 10, ****p < 0.0001). (C, D) Catalase (CAT) and superoxide dismutase (SOD) activities as representative endogenous antioxidant enzymes in the cerebral cortex (n = 10, *p < 0.05, ***p < 0.001, ****p < 0.0001).

Figure 4. HVSS preserves hippocampal structure and neuronal integrity. (A) Representative images of hippocampal DG regions and quantitative analyses of CA1-CA3 thickness (arrows) and cellular density in the DG region (n = 10, **p < 0.01, ***p < 0.001, ****p < 0.0001). The scale bar represents 320 □m. (B) Representative images and quantification of cleaved caspase-3-positive apoptotic cells (red, arrows) in the DG region (n = 10, ****p < 0.0001). Cleaved caspase-3 positive cells were quantified as the number of cells per square millimeter (cells/mm^2) within defined hippocampal regions. Scale bar represents 160 □m. (C) Representative images and quantification of c-Fos positive activated cells (red, arrows) in the DG region (n = 10, ****p < 0.0001). c-Fos positive cells were quantified as the number of cells per square millimeter (cells/mm^2) within defined

hippocampal regions. Scale bar represents 160 □m.

Figure 5. HVSS upregulates hippocampal memory-related signaling genes. Relative mRNA expression levels of (A) brain-derived neurotrophic factor (*BDNF*), (B) phosphoinositide 3-kinase (*PI3K*), (C) *AKT*, (D) extracellular signal-regulated kinase 1 (*ERK1*), (E) *ERK2*, (F) cAMP response element-binding protein (*CREB*), and (G) calcium/calmodulin-dependent protein kinase 4 (*CAMK4*) were measured by qRT-PCR (n=10, ****$p < 0.0001$).

Supplementary figure legends

Supplementary figure 1. Body weight remained stable throughout the experimental period. Body weight changes in vehicle, SCP, and HVSS-treated mice (20, 40, and 80 Hz) during the 28-day stimulation period. Measurements were taken on days -1, 0, 1, 6, 13, 20, 27, and 28. No significant differences were observed among groups at any time point, indicating that HVSS did not affect general health or growth (n = 20).

Supplementary figure 2. HVSS did not alter gross brain morphology. Representative images of whole brains from (A) Vehicle, (B) SCP, (C) HVSS-20 Hz, (D) HVSS-40 Hz, and (E) HVSS-80 Hz treated mice. No discernible differences in gross brain morphology were observed among groups.

Supplementary figure 3. Adrenal gland morphology was unaffected by HVSS. Representative images of adrenal glands from (A) Vehicle, (B) SCP, (C) HVSS-20 Hz, (D) HVSS-40 Hz, and (E) HVSS-80 Hz treated mice. No apparent morphological alterations were detected among groups.

Supplementary figure 4. HVSS did not induce histopathological alterations in adrenal glands. Representative histopathological images of adrenal glands from vehicle, SCP, and HVSS (20, 40, and 80 Hz) treated mice. The were no significant differences in overall gland thickness, medulla, or cortical layers (zona glomerulosa, zona fasciculate, and zona reticularis).

Supplementary figure 5. HVSS did not affect serum corticosterone levels. Serum corticosterone concentrations in vehicle, SCP, and HVSS-treated mice (20, 40, and 80 Hz). No significant group differences were observed, indicating that HVSS did not induce stress-related endocrine alterations (n = 10, ns: not significant).

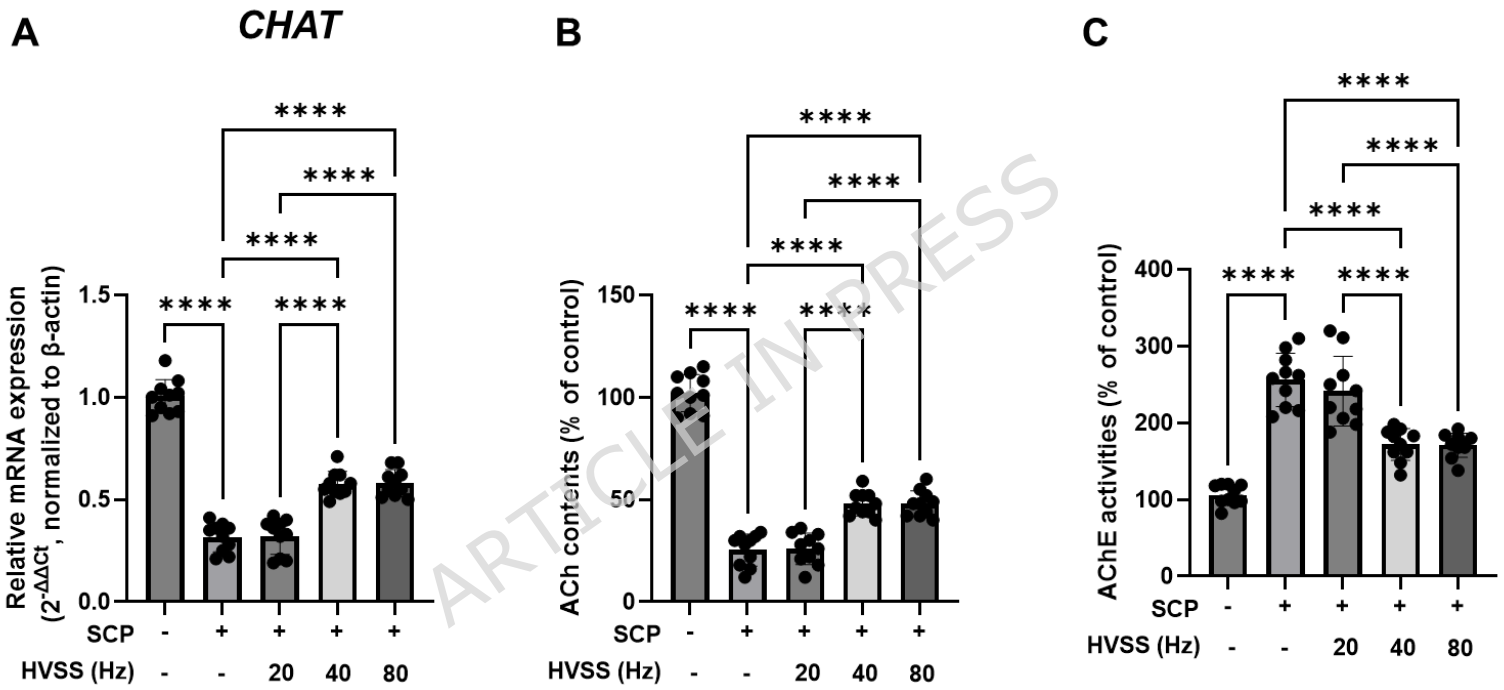

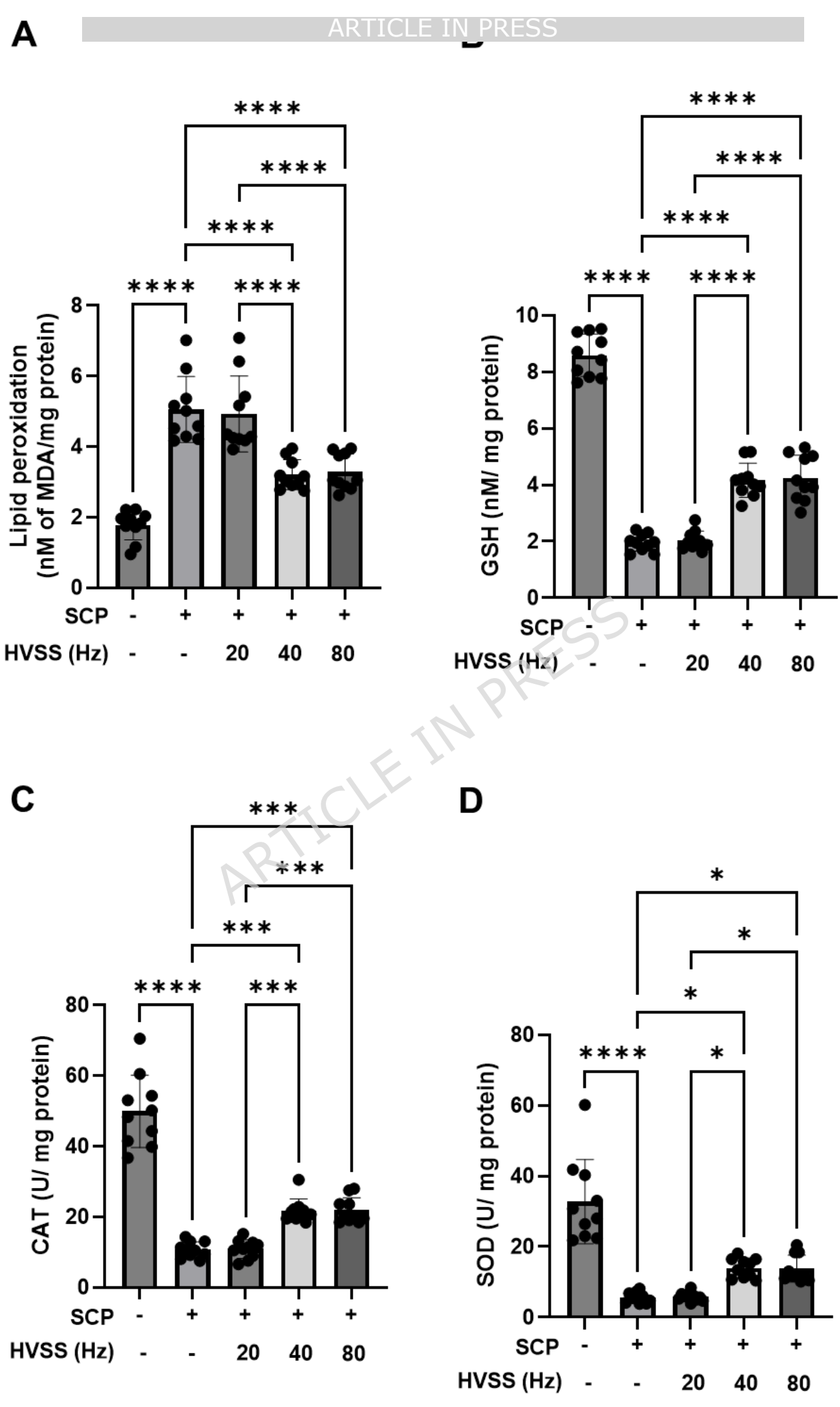

A

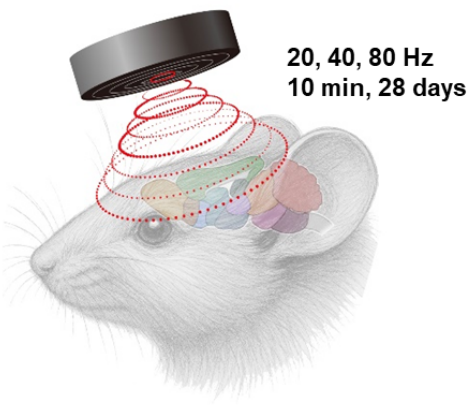

B

Test Eqiuipment = Head-mounted Vibrotactile Stimulation System for mouse (HVSS)

C

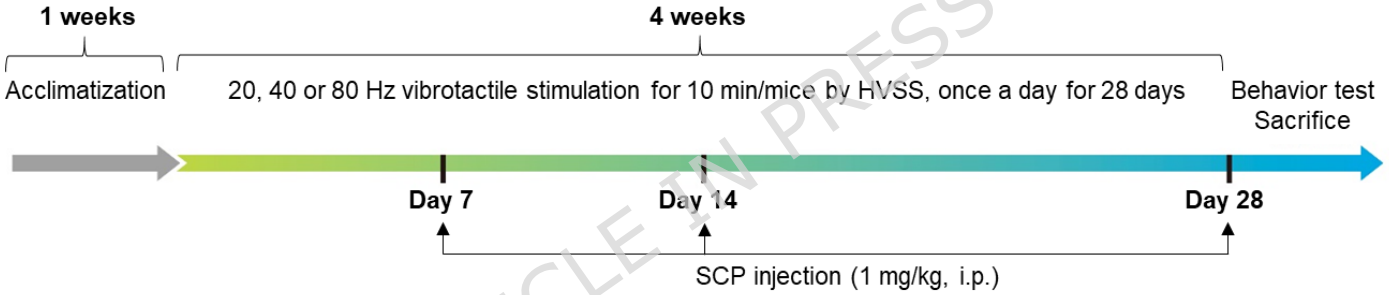

D

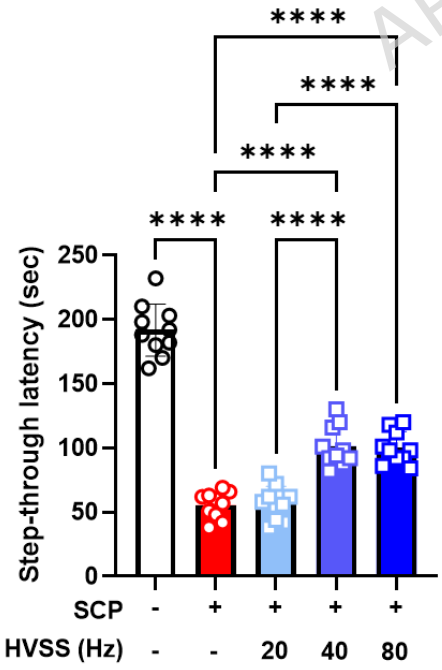

E

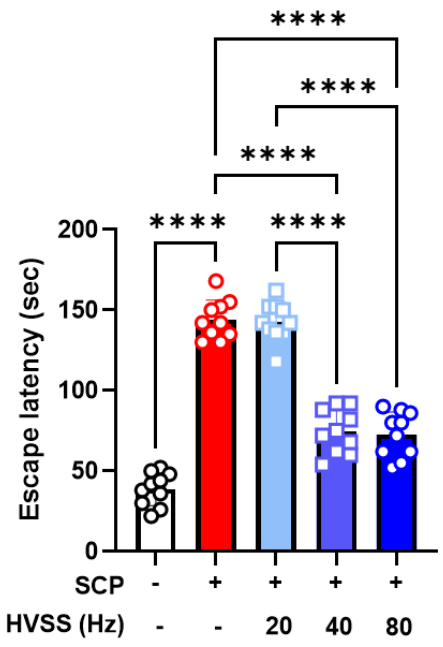

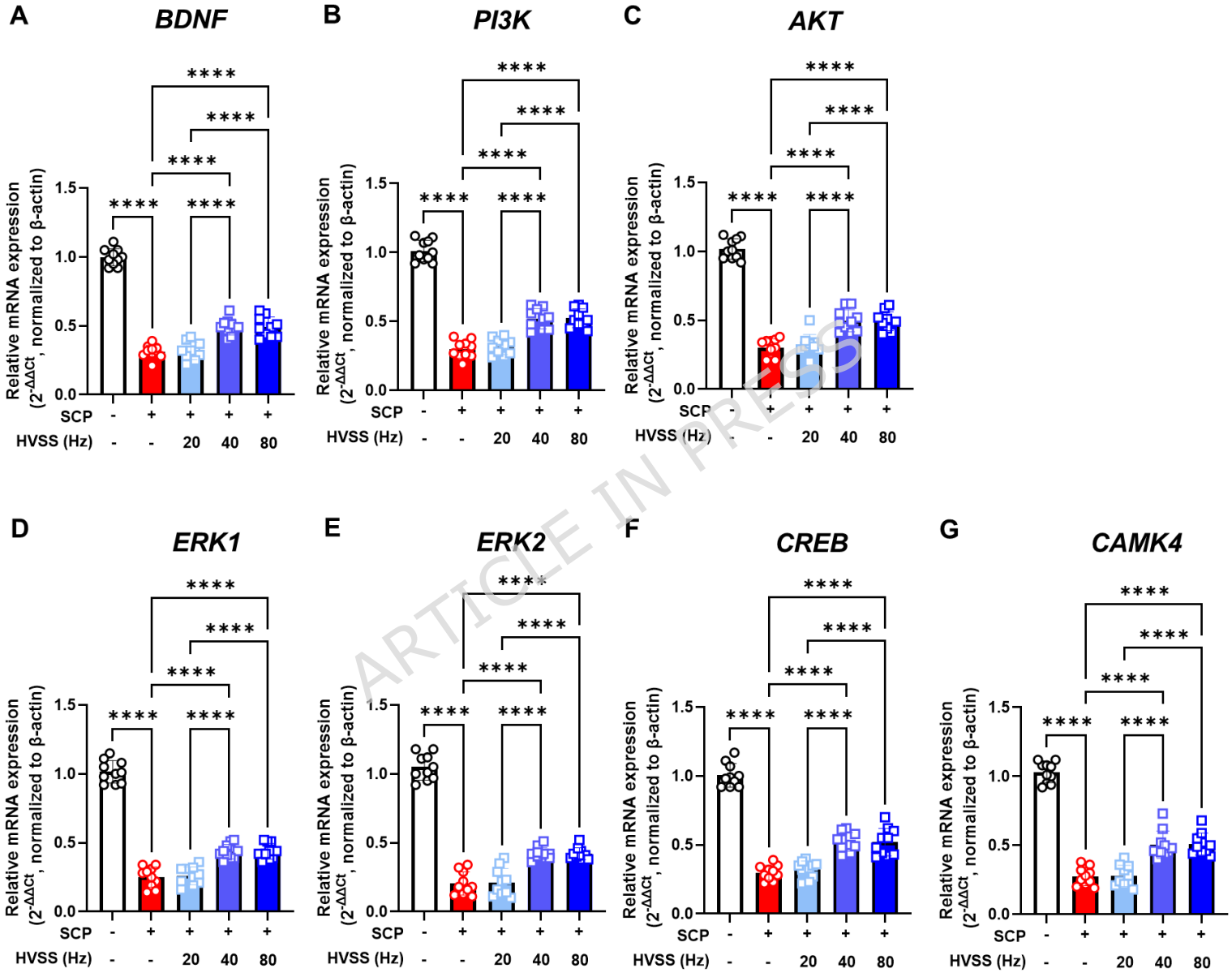

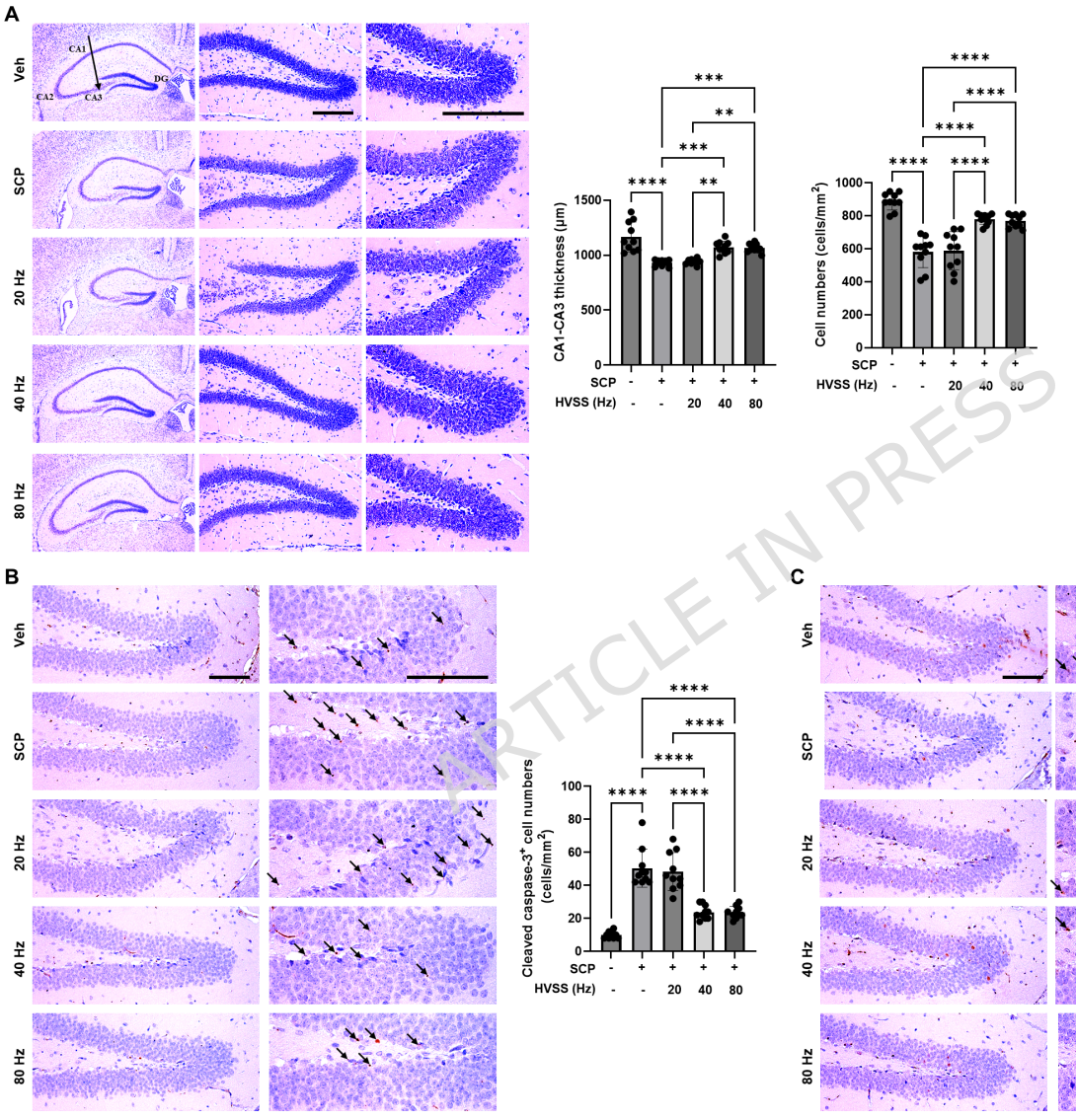

Table 1. Oligonucleotides for qPCR

Target	5’ – 3’	Sequence	NCBI Accession Number
ChAT	Sense	GCTTGAATGGAGCGAATCGTTGG	NM_009891
	Antisense	CACCAGGACGATGCCATCAAAAG	
BDNF	Sense	GGCTGACACTTTTGAGCACGTC	NM_007540
	Antisense	CTCCAAAGGCACTTGACTGCTG	
PI3K	Sense	CAAACCACCCAAGCCCACTACT	NM_001077495
	Antisense	CCATCAGCAGTGTCTCGGAGTT	
AKT	Sense	GGACTACTTGCACTCCGAGAAG	NM_009652
	Antisense	CATAGTGGCACCGTCCTTGATC	
ERK1	Sense	GGCTTTCTGACGGAGTATGTGG	NM_011952
	Antisense	GTTGGAGAGCATCTCAGCCAGA	
ERK2	Sense	TCAAGCCTTCCAACCTCCTGCT	NM_001038663
	Antisense	AGCTCTGTACCAACGTGTGGCT	
CREB	Sense	CACAGACCACTGATGGACAGCA	NM_009952
	Antisense	AGGACGCCATAACAACTCCAGG	
CAMK4	Sense	GGAGAAGGGATACTACAGTGAGC	NM_009793
	Antisense	CTGGTTTGAGGTCACGATGGAC	
β-actin	Sense	CATTGCTGACAGGATGCAGAAGG	NM_007393
	Antisense	TGCTGGAAGGTGGACAGTGAGG	

qPCR = quantitative reverse transcription polymerase chain reaction; NCBI = National Center for Biotechnology Information; ChAT = choline acetyltransferase; BDNF = brain-derived neurotrophic factor; PI3K = phosphoinositide 3-kinase; AKT = protein kinase B; ERK = extracellular signal–regulated kinase; CREB = cAMP response element-binding protein; CAMK = calcium/calmodulin-dependent protein kinase

All primer pairs were obtained from OriGene Technologies (Rockville, MD, USA).

Table 2. Primary Antibodies and Detection Kits Used for Immunohistochemical Analysis

Antibody/detection kit	Catalogue number	Source	Dilution
Primary antibody			
Anti-cleaved caspase-3 (Asp175) antibody	9661	Cell Signaling Technology Inc, Beverly, MA, USA	1:400
Anti-c-Fos antibody [EPR21930-238]	ab222699	Abcam, Cambridge, UK	1:2,000
Detection kits			
Vectastain Elite ABC kit	PK-6200	Vector Lab., Burlingame, CA, USA	1:50
Peroxidase substrate kit	SK-4100	Vector Lab., Burlingame, CA, USA	1:50

All antibodies were diluted in 0.01 M phosphate buffered saline (pH 7.2).

ABC = avidin-biotin-peroxidase complex